Part III. Nucleation and growth
Module 4 : Growth of precipitates and kinetics of nucleation and growth

4.1 Motivating question/phenomenon

In Figure. 20 we show, schematically, a morphology of precipitates known as the Widmanstätten ferrite lath morphology; there are two austenite (fcc phase of a solid solution of iron and carbon) grains, namely γ_1 and γ_2; the α (ferrite – a bcc solid solution of iron and carbon) phase nucleates at the grain boundary that separates the two γ grains; it grows into one of the γ phases as a lath. The schematic shows both the side view and the top view of these ferrite laths. What is the reason for the formation of Widmanstätten morphology?

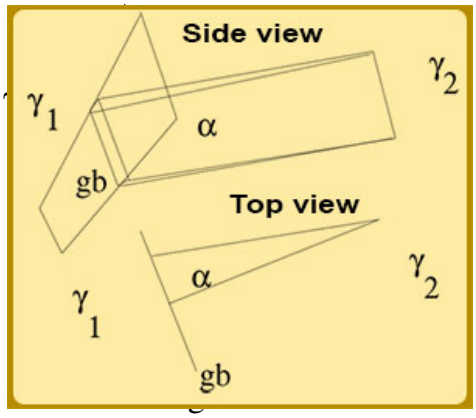

Figure 20: A schematic (side and top) view of the Widmanstätten ferrite lath morphology. The top figure is the side view and the bottom one is the top view.

In Figure. 21, we show a particular morphology of β precipitate seen at the interface between two grains of another phase (say, α); this morphology is known as grain-boundary allotriomorph. What is the reason for the formation of such allotriomorphs?

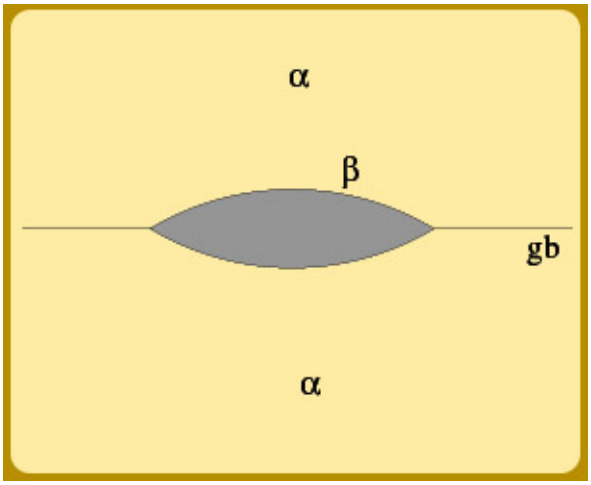

Figure 21: A schematic view of grain-boundary allotriomorph.

4.2 Precipitate growth kinetics: Diffusion limited growth of a planar, incoherent precipitate-matrix boundary

Consider an alloy of composition c_0 which is cooled from a high temperature into a two phase region as shown in Figure. 22. At this temperature, the alloy phase separates into two phases, say, α and β, with equilibrium compositions given by c_e^β and c_e^α. Let us consider the phase separation that takes place by the nucleation and growth mechanism. Suppose the β phase has nucleated and is growing into the supersaturated α phase; we assume that the α-β boundary is planar and incoherent. Our aim, in this section, is to calculate the velocity of such a planar, incoherent boundary using an approximate method due to Zener (Theory of growth of spherical precipitates from solid solution, C. Zener, Journal of Applied Physics, Vol. 20, pp. 950-953, 1949).

In Figure. 22 we also show, schematically, the microstructure; the two phases β and α are separated by a planar interface. We also show the composition profile as we go from the precipitate into the superaturated matrix. The composition of the β phase is c_e^β as given by the phase diagram. However, on the α side the composition is not a constant. On the α side, at the interface, the composition of the α phase is c_e^α as given by the phase diagram. Far from the α-β interface, the composition of the α phase is the same as the initial alloy composition, namely, c_0. In the middle region, the composition changes from c_e^α to c_0 in a continuous manner. This composition profile is

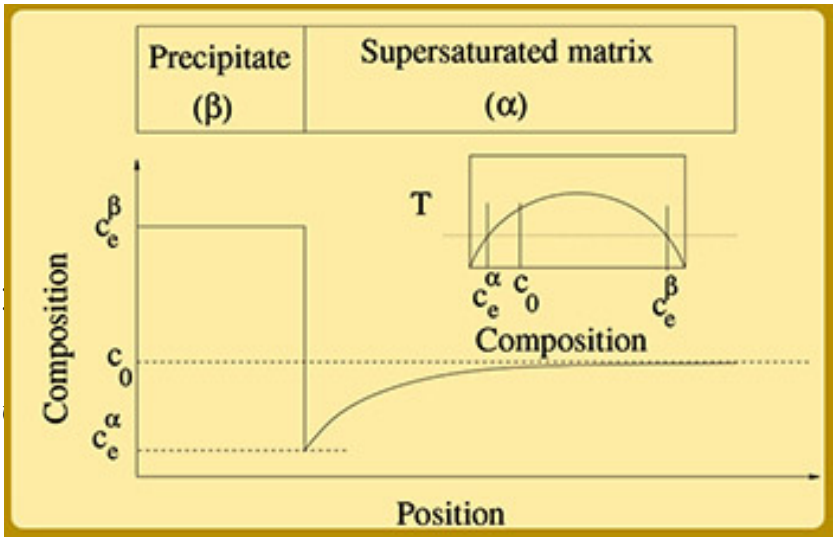

Figure 22: Schematic of an incoherent β precipitate with planar boundary growing into a supersaturated α phase.

schematically shown in the Figure. 22; this profile results due to the diffusion of B atoms in the α phase.

Consider a unit cross-section of the α-β interface which moves a small distance, say, dx in a given time, say, dt. The number of B atoms needed for such a movement of the interface is given by $(c_e^\beta - c_e^\alpha)dx$. Since these B atoms are supplied to the interface by diffusion, using the Fick's first law, one can calculate the number of B atoms that diffuse in time dt as $D\left(\frac{dc}{dx}\right)dt$ where D is the interdiffusion coefficient. Equating these two quantities, one can obtain the velocity of movement v of the interface as follows:

$$v = \frac{dx}{dt} = \frac{D}{(c_e^\beta - c_e^\alpha)}\frac{dc}{dx} \tag{51}$$

As the precipitate grows, $\frac{dc}{dx}$ keeps decreasing – and hence, more and more of the matrix regions participate in the diffusion process to supply B atoms to grow the precipitate. As noted earlier, Zener introduced a simplified profile to calculate the velocity approximately. This simplified profile is shown in Figure. 23. From the profile, clearly, $\frac{dc}{dx} = \frac{c_0 - c_e^\alpha}{L} = \frac{\Delta C_0}{L}$. The value of L can be calculated using conservation of B atoms, which demands that the shaded rectangle on the left is equal in area to the shaded triangle on the

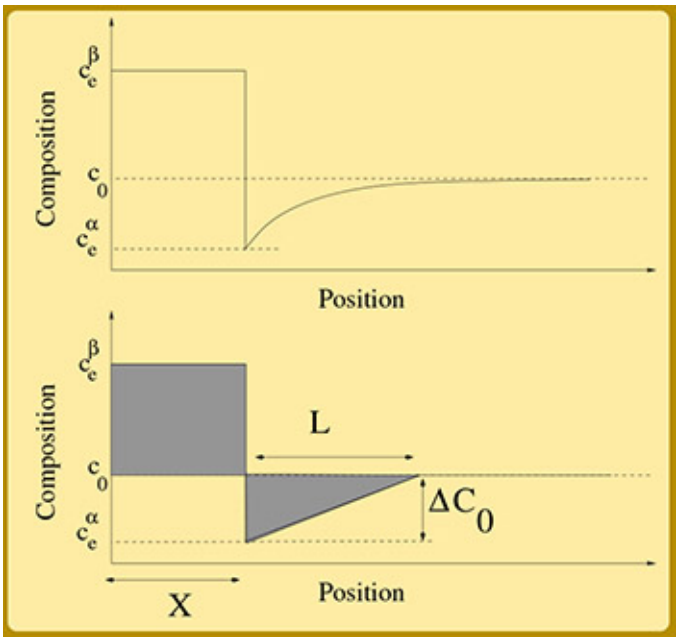

Figure 23: the Zener approximation to calculate the growth velocity of a planar, incoherent precipitate-matrix boundary.

right. Hence,

$$\frac{1}{2}\Delta c_0 L = x(c_e^\beta - c_0); \tag{52}$$

Thus,

$$L = \frac{2x(c_e^\beta - c_0)}{\Delta c_0}. \tag{53}$$

Substituting Eq. 53 in Eq. 51, we obtain

$$v = \frac{dx}{dt} = \frac{D}{(c_e^\beta - c_e^\alpha)} \frac{(\Delta c_0)^2}{2x(c_e^\beta - c_0)} = \frac{D(\Delta c_0)^2}{2x(c_e^\beta - c_e^\alpha)(c_e^\beta - c_0)} \tag{54}$$

Further simplifications are possible if we assume that the molar volumes of both the phases are the same – in which case, we can replace the concentrations by mole fractions (X = C V_m). Also, we can assume, for the sake of simplicity, $(c_e^\beta - c_0) = (c_e^\beta - c_e^\alpha)$ - that is, we consider a case in which the far-field composition is very small. Thus, we obtain,

$$v = \frac{dx}{dt} = \frac{D(\Delta X_0)^2}{2x(X_e^\beta - X_e^\alpha)^2}. \tag{55}$$

The expression in Eq. 55 can be integrated to obtain

$$x = \frac{\Delta X_0}{(X_e^\beta - X_e^\alpha)}(\sqrt{Dt}). \tag{56}$$

Note that in the above equation (and for the rest of this module) we assume that at the initial time $t_0 = 0$.

Now, the expression in Eq. 56 can be differentiated to obtain the velocity as

$$v = \frac{\Delta X_0}{2(X_e^\beta - X_e^\alpha)} \left(\sqrt{\frac{D}{t}}\right). \tag{57}$$

4.3 Consequences of Eq. 56 and 57

Let us consider Eq. 56:

$$x = \frac{\Delta X_0}{(X_e^\beta - X_e^\alpha)}(\sqrt{Dt}). \tag{58}$$

This equation shows that the distance to which the interface moves is proportional to $\sqrt{Dt}$. In other words, the thickeninng of the precipitate is parabolic. As we have seen earlier such a parabolic growth is a common feature of all diffusion limited growth. Although this conclusion is derived under simplifying assumptions, more thorough treatments and allowing for curved boundaries do not change this conclusion: the linear dimensions of a spheroidal precipitate increases as $\sqrt{Dt}$ as long as the interface migration is diffusion controlled.

Let us consider Eq. 57:

$$v = \frac{\Delta X_0}{2(X_e^\beta - X_e^\alpha)} \left(\sqrt{\frac{D}{t}}\right). \tag{59}$$

This equation shows that the velocity of the interface is proportional to $\sqrt{\frac{D}{t}}$ as well as to ΔX_0 (the supersaturation at the beginning of the precipitation).

From the phase diagram, it is clear that ΔX_0 increases with increasing supersaturation. Thus, as undercooling increases, the velocity of the precipitate-matrix interface should increase. However, the diffusivity is high at high

temperatures and low at lower temperatures. In other words, the diffusivity gives lower velocities at higher undercoolings. Hence, the velocity of the precipitate-matrix interface is high at intermediate undercooling as shown in Fig. 24.

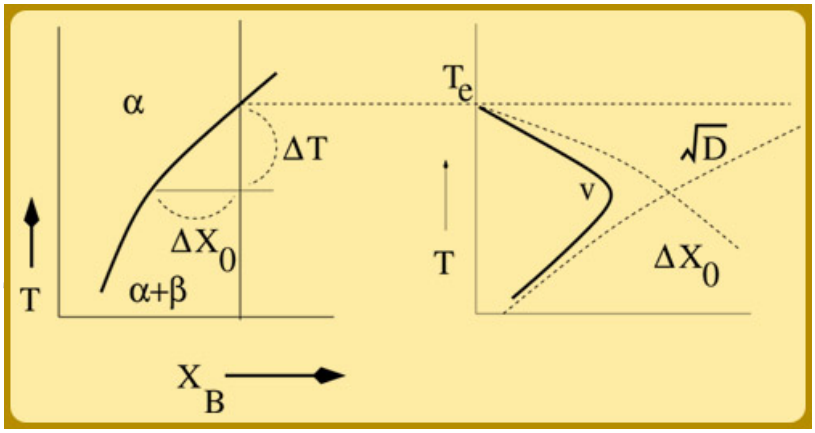

Figure 24: The velocity change with undercooling; the velocity is maximum at intermediate undercooling because at high undercoolings diffusivity is high but supersaturation is low, whereas at low undercooling diffusivity is low but supersaturation is high.

4.4 Interface structure and growth

The structure of an interface has a strong say in its growth rate. In general, the low energy, coherent and semi-coherent boundaries have low mobility; the high energy, incoherent boundaries have high mobilities. So, if a precipitate (say, of β phase) shares a coherent (or semi-coherent) boundary and an incoherent boundary with two different grains (say, of α phase) as shown in Fig. 25, then, in general, the incoherent interface will grow at a faster velocity than the coherent interface (as indicated). Such differences in the growth rates of different interfaces of a precipitate can result in interesting precipitate morphologies; the Widmanstätten morphology is in fact, a result of such differing movement of different parts of the precipitate-matrix interface.

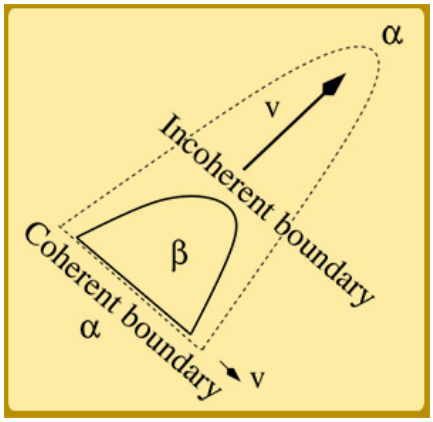

Figure 25: The interface structure and growth; in general, coherent boundaries have low mobility and incoherent ones have high mobilities.

4.5 Diffusion limited lengthening of plates/needles

Consider, for example, the growth of a platelike precipitate with coherent facetted faces and incoherent edges. In such a case, it is possible that the thickness of the plate would remain constant while the cylindrically curved edge would grow. In Fig. 26 we show the growth of such a precipitate along with the composition profile. One important change in the composition profile as compared to the one in Fig. 22 is that the composition on the matrix side is not the equilibrium composition given by the phase diagram but is elevated due to Gibbs-Thomson effect.

In this case also, an equation similar to Eq. 51 holds (with the composition on the α side of the interface corrected for Gibbs-Thomson):

$$v = \frac{dx}{dt} = \frac{D}{c_e^{\beta} - c_r} \frac{dc}{dx} \tag{60}$$

As earlier, assuming equal molar volumes for both the phases, it can be shown that

$$\frac{dc}{dx} \approx \frac{\Delta X_0}{kr} \left(1 - \frac{r^\star}{r}\right) \tag{61}$$

where, k is a constant of order unity and $r^\star$ is the radius of critical nucleus, that is, the radius for which ΔX is reduced to zero. Thus, we get, for the

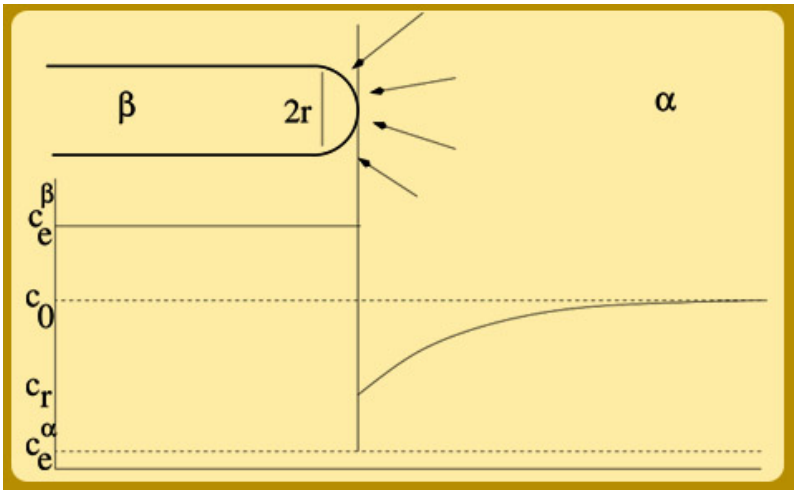

Figure 26: Diffusion limited lengthening of a plate of constant thickness; note the Gibbs-Thomson effect on composition at the curved interface on the α side.

plate/needle lengthening velocity as

$$v = \frac{D}{X_e^\beta - X_r} \frac{\Delta X_0}{kr} \left(1 - \frac{r^\star}{r}\right) \tag{62}$$

An important consequence of such an expression as above is that the diffusion limited plate lengthening rate, for a given thickness of the plate, is a constant; that is, $x \propto t$; in other words, the rate of growth is linear.

4.6 Ledge growth of facetted interfaces

The facetted interfaces usually grow by ledge mechanism. Consider the schematic of a facet growing by the ledge mechanism (Fig. 27). The facet grows a distance ℓ by the movement of the step of height h. If the step moves at a velocity of u, the velocity of the interface normal to itself is given by v, and,

$$v = \frac{uh}{\ell} \tag{63}$$

In this case also, as in Eq. 62, we can obtain the lengthening rate u (by

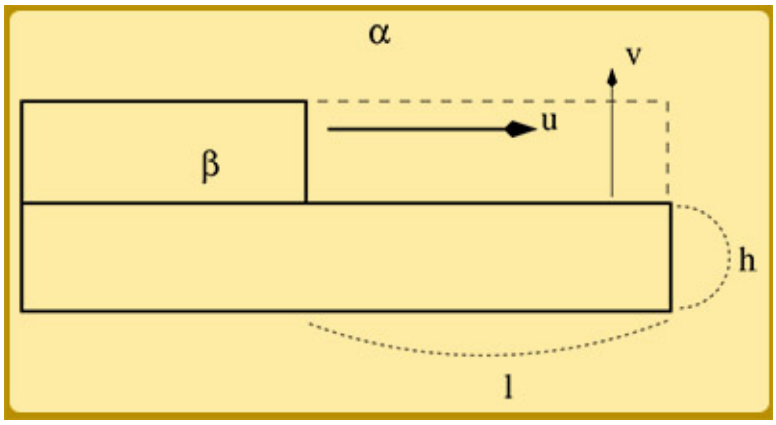

Figure 27: The growth of a facet by ledge mechanism. The ledge grows laterally at a velocity of u, for a distance ℓ; the height of the ledge is h. Due to the growth of the ledge, the facet thickens (grows normal to itself) at a velocity of v.

replacing r by h, and not incorporating the Gibbs-Thomson correction)

$$u = \frac{D}{X_e^\beta - X_e} \frac{\Delta X_0}{kh}. \tag{64}$$

Thus, the ledge growth rate is obtained as

$$v = \frac{D}{X_e^\beta - X_e} \frac{\Delta X_0}{k\ell} \tag{65}$$

4.7 TTT diagrams and JMAK kinetics

The overall nucleation and growth kinetics are generally represented, for isothermal transformations, using the TTT (Time-Temperature-Transformation) diagrams. In Fig. 28 we show a schemamtic TTT diagram; the time and temperature are plotted in the x and y-axes respectively; the beginning and ending of transformations are drawn (by arbitrarily taking 1 and 99% transformation as the beginning and ending of the transformation respectively). As shown, the typical TTT diagrams are C curves; in terms of time versus fraction transformed, these are the so called S curves as shown in Fig. 28. The C-curve indicates that the incubation time, that is the time taken for the transformation to start at every temperature is the lowest at intermediate temperatures. This is because, as we discussed in this module and the

previous one, both the nucleation and growth kinetics are faster at the intermediate temperatures; at low undercoolings (high temperatures), the driving forces for the transformation are very low making the kinetics to be slower; at high undercoolings (low temperatures), on the other hand, the diffusional kinetics is very slow making the overall transformation kinetics to be very slow. Finally, the S curves of the type shown in Fig. 28 can be understood in terms of what is known as the Johnson-Mehl-Avrami-Kolmogorov (JMAK) kinetics; see the supplementary information at the end of this module for a derivation of the JMAK kinetics.

4.8 Tutorial problems and questions

1. The incoherent planar boundary that separates a precipitate and matrix thickens as

   (a) $\sqrt{Dt}$

   (b) $\sqrt{\frac{D}{t}}$

   (c) Dt

   (d) $\frac{D}{t}$

2. With increasing undercooling, the velocity of a precipitate-matrix interface

   (a) increases and hence peaks at highest undercooling

   (b) decreases and hence peaks at lowest undercooling

   (c) increases and then decreases and hence peaks at intermediate undercooling

   (d) decreases and then increases and hence peaks at both highest and lowest udercoolings

3. The migration rate of an incoherent, planar precipitate-matrix interface is proportional to

   (a) ΔX_0

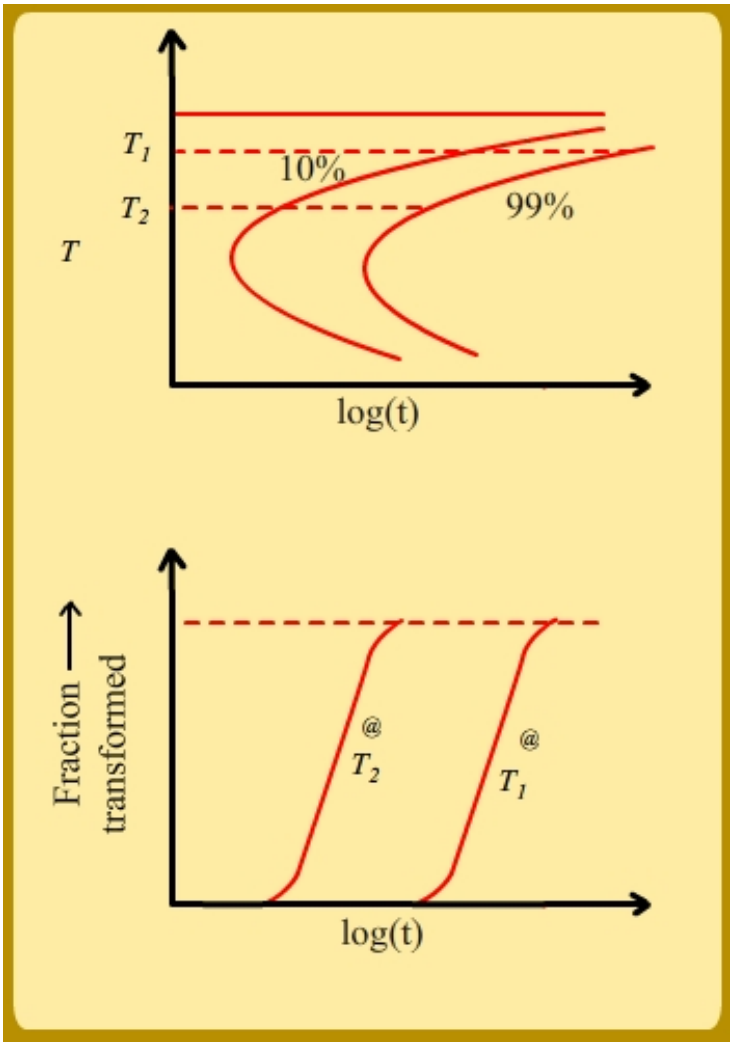

Figure 28: The TTT diagram (C curves) and the fraction transformed as a function of time at different temperatures (S curves).

(b) $(\Delta X_0)^2$

(c) $\frac{1}{\Delta X_0}$

(d) $\frac{1}{(\Delta X_0)^2}$

4. In general,

   (a) the mobilities of coherent and incoherent boundaries are the same

   (b) the mobility of coherent boundary is lower than that of incoherent boundary

   (c) the mobility of incoherent boundary is lower than that of coherent boundary

5. Derive Eq. 56 from Eq. 55 by integration, and Eq. 57 from Eq. 56 by differentiation.

6. Consider the phase diagram shown in Fig. 29. Let T1, T2 and T3 be 1000, 650 and 600 K, respectively. Consider two pieces of an alloy of composition 0.25; let one be cooled from T1 to T2 and kept at T2 for about 2 minutes while the other is cooled from T1 to T3 and kept at T3 for about 2 minutes. Assuming incoherent and planar boundary between β nuclei and supersaturated α phase, calculate the increase in length of the precipitates in these two cases. The relevant diffusivity data is as follows: $D_0 = 1.2 \text{ x } 10^{-2} m^2/sec$ and Q = 150 kJ/mol.

7. Consider the growth of two precipitates which are close to each other as shown in the schematic (Fig. 30). Can Eq. 57 be used to describe the growth of these two precipitates? Explain.

8. Consider the growth of a β precipitate nucleated at the grain boundary of two α grains. Explain the growth of such a precipitate assuming that the solute diffuses substitutionally. Would the growth process be different if the solute diffuses interstitially?

4.9 Solutions to the tutorial

1. (a) $\sqrt{Dt}$

   The growth is parabloic.

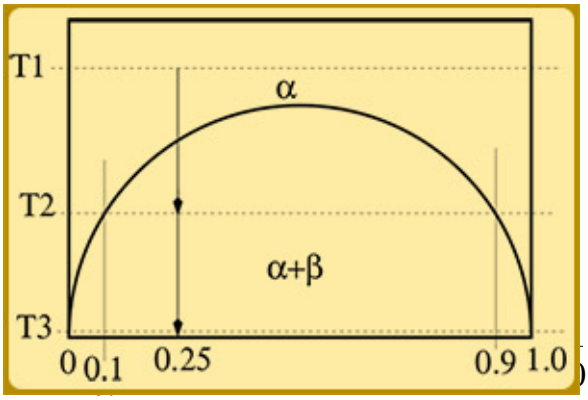

Figure 29: Schematic phase diagram to show the heat treatment. The overall alloy composition is 0.25. In one case, the alloy is cooled from T1 to T2 and is kept at T2 for 5 hours. In the other, the alloy is cooled from T1 to T2 and is kept at T3 for 5 hours.

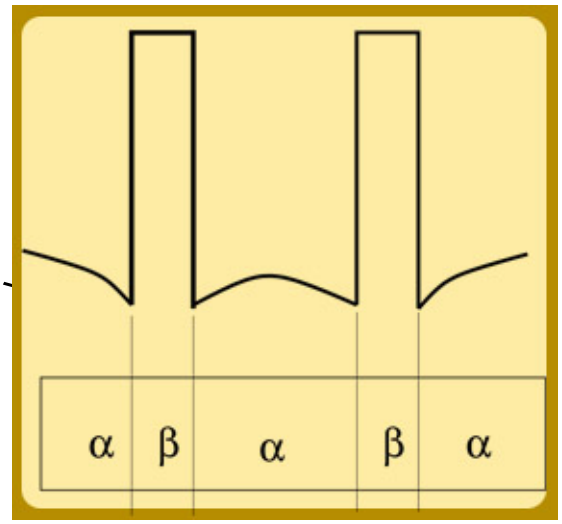

Figure 30: Two β precipitates close to each other in a supersaturated α matrix growing with planar, incoherent boundaries.

2. (c) increases and then decreases and hence peaks at intermediate undercooling.

   See Fig. 24

3. (a) ΔX_0

   See. Eq. 57.

4. (b) the mobility of coherent boundary is lower than that of incoherent boundary

5. Consider Eq. 55

$$v = \frac{dx}{dt} = \frac{D(\Delta X_0)^2}{2x(X_e^\beta - X_e^\alpha)^2}. \tag{66}$$

$$2xdx = \frac{D(\Delta X_0)^2}{(X_e^\beta - X_e^\alpha)^2} dt. \tag{67}$$

$$x^2 = \frac{D(\Delta X_0)^2}{(X_e^\beta - X_e^\alpha)^2} t. \tag{68}$$

$$x = \frac{(\Delta X_0)}{(X_e^\beta - X_e^\alpha)} \sqrt{Dt}. \tag{69}$$

This is Eq. 56. To obtain Eq. 57, let us start with the above equation and differentiate it with respect to time:

$$x = \frac{(\Delta X_0)}{(X_e^\beta - X_e^\alpha)} \sqrt{D} t^{\frac{1}{2}}. \tag{70}$$

$$v = \frac{dx}{dt} = \frac{(\Delta X_0)}{(X_e^\beta - X_e^\alpha)} \sqrt{D} \frac{1}{2t^{\frac{1}{2}}}. \tag{71}$$

Thus, we obtain the Eq. 57:

$$v = \frac{dx}{dt} = \frac{(\Delta X_0)}{2(X_e^\beta - X_e^\alpha)} \left(\sqrt{\frac{D}{t}} \right). \tag{72}$$

6. We know that the increase in length is given by

$$x = \frac{(\Delta X_0)}{(X_e^\beta - X_e^\alpha)}\sqrt{Dt}. \tag{73}$$

Here, $\sqrt{Dt}$ is known as the diffusion distance. This distance is temperature dependent because D is temperature dependent. Hence, let us calculate the diffusion distance at T2 and T3. Given: D_0 = 1.2 x 10^{-2}m^2/sec and Q = 150 kJ/mol. Also, $D = D_0 \exp(-Q/RT)$ where R is the universal gas constant.

Hence, D (T2 = 650K) = $1.2 \times 10^{-2} \exp -150000/(8.314 * 650) = 1.06$ x 10^{-14} and, D(T3= 600K) = 1.05 x 10^{-15}. Thus, the diffusion distance at 650 K is nearly 14 microns while it is about 4 microns at 600 K.

ΔX_0 is 0.15 (that is, 0.25-0.1) 650 K and 0.25 (that is, 0.25-0) at 600 K. Further, $X_e^\beta - X_e^\alpha$ is 0.8 (that is, 0.9-0.1) at 650 K, and is 1.0 (that is, 1.-0.) at 600 K.

Hence, at 650 K, the growth is about 2.6 microns while at 600 K, the growth is about 1.1 microns.

7. No; we have derived Eq. 57 by assuming certain $\frac{dc}{dx}$. However, when two precipitates are close, their diffusion fields overlap. Because of this, the $\frac{dc}{dx}$ decreases much more rapidly then when there is only one precipitate. So, in the case where the diffusion fields overlap, the growth rate decelerates much more rapidly and hence the growth rate deviates from that given by Eq. 57.

8. In the case of substitutional solute, the grain boundary diffusion is relatively faster than bulk diffusion. So, from the bulk, B atoms diffuse to the grain boundary from which they diffuse along the precipitate-matrix boundary to form a lens shaped precipitate. Such rapid lengthening and thicknening of the precipitate, however, is not important in the case of interstitial solutions in which both the grain boundary and bulk diffusivities are comparable.

5.0 Supplementary information

The JMAK kinetics is derived in [2]; we outline the mathematical steps here and refer the interested reader to [2].

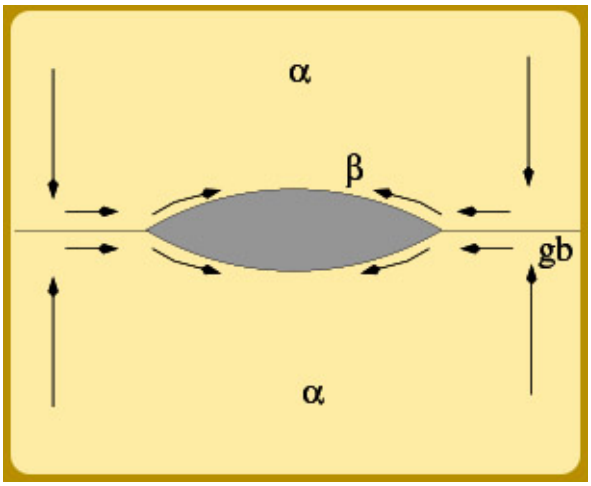

Figure 31: Short circuit diffusion and the resultant precipitate morphology.

Assuming spherical particles, a nucleation rate of N, and a growth rate of V, the volume fraction of transformed phase (X) at time $t = \tau$ can be shown to obey the differential equation

$$\frac{dX}{1-X} = \frac{4}{3}\pi V^3 (t-\tau) N d\tau \tag{74}$$

Integrating this equation, one obtains the JMAK kinetics, namely,

$$X = 1 - \exp\left(-\frac{\pi}{3} N V^3 t^4\right) \tag{75}$$

There are cases wherein JMAK kinetics might fail; one such case is the crystallization kinetics in certain polymers. The modification to JMAK in such cases is discussed in greater detail in [3].

References

[1] David A. Porter, Kenneth E. Easterling, and Mohamed Y. Sherif, Phase transformations in metals and alloys, CRC press, Third edition, 2009.

[2] V Raghavan, Solid state phase transformations, Prentice-Hall India Pvt. Ltd., First edition, 1992.

[3] Reinhard Illner, C Sean Bohun, Samantha McCollum, and Thea van Roode, Mathematical modelling: a case studies approach, Vol. 27, Student Mathematical Library, Indian Edition, American Mathematical Society, 2011.